MOL #60111

Identification of determinants of glucose-dependent insulinotropic polypeptide receptor that interact with N-terminal biologically active region of the natural ligand

Tahir Yaqub, Irina G. Tikhonova, Jens Lättig, Remi Magnan, Marie Laval, Chantal Escrieut, Cyril Boulègue, Chandralal Hewage and Daniel Fourmy

 INSERM, Institut national de la santé et de la recherche médicale, Unit U858, Toulouse, France; Université Paul Sabatier (Toulouse III), Toulouse, France (TY, IGT, JL, RM, ML, CE, DF)

Max-Planck-Institut für Biochemie, D-82152 Martinsried, Germany (CB)

Conway Institute, University college Dublin, Dublin, Ireland (CH)

Running title: agonist activation site of GIPR

Daniel Fourmy, U858 INSERM I2MR, equipe 13, 1 avenue Jean Poulhès, BP 84225, 31432 Toulouse Cedex 4, France. Email: Daniel.Fourmy@inserm.fr

Number of text pages: 31

Number of tables: 1

Number of figures: 10

Number of references: 38

Number of words: 8919

Abstract: 249

Introduction: 670

Discussion: 1477

Non-standard abbreviations used: GIP, glucose-dependent insulinotropic polypeptide; GIPR: glucose-dependent insulinotropic polypeptide receptor; GPCR, G-protein coupled receptors

Abstract: Glucose-dependent insulinotropic polypeptide receptor (GIPR), a member of family B of G-protein coupled receptors, is a potential therapeutic target for which discovery of non peptide ligands is highly desirable. Structure-activity relationship studies indicated that the N-terminal part of GIP is crucial for biological activity. Here, we aimed at identification of residues in the GIPR involved in functional interaction with N-terminal moiety of GIP. Homology model of the transmembrane core of GIPR was built whereas 3-D model of the complex formed between GIP and N-terminal extracellular domain of GIPR was taken from crystal structure. The later complex was docked to the transmembrane domains of GIPR allowing *in silico* identification of putative residues of the agonist binding/activation site. All mutants were expressed at the surface of HEK 293 cells as indicated by flow cytometry and confocal microscopy analysis of fluorescent GIP binding. Mutation of residues Arg183, Arg190, Arg300 and Phe357 caused shifts of 76-, 71-, 42- and 16-fold in the potency to induce cAMP formation, respectively. Further characterization of these mutants, including tests with alanine substituted GIP analogues, are in agreement with interaction of Glu3 in GIP with Arg183 in GIPR. Furthermore, they strongly supported a binding mode of GIP to GIPR in which the N-terminal moiety of GIP was sited within transmembrane helices 2, 3, 5, and 6 with biologically crucial Tyr1 interacting with Gln224 (TMH3), Arg300 (TMH5) and Phe357 (TMH6). These data represent an important step towards understanding activation of GIPR by GIP which should facilitate the rational design of therapeutic agents.

Glucose-dependent insulinotropic polypeptide (Gastric inhibitory polypeptide, GIP) is a 42 residue hormone released by the entero-endocrine K cells lining the proximal duodenum (Jornvall et al., 1981; Moody et al., 1984). GIP stimulates insulin secretion from pancreatic β-cells after ingestion of nutrients. The peptide has a very short half life in the blood as it is vulnerable to degradation by ubiquitous enzyme dipeptidyl peptidase IV (Mentlein et al., 1993). GIP along with its sister incretin hormone Glucagon-like peptide 1 (GLP1) has been shown to account for 50 to 70 percent of post-prandial insulin secretion. The incretin effect is strictly glucose-dependent and is essential for the maintenance of glucose homeostasis. GIP further enhances its glucose-lowering effects by the inhibition of hepatic glucose production and the stimulation of proinsulin gene transcription and translation. Due to its hypoglycemic and hypolipidemic effects (Baggio and Drucker, 2007; Brown, 1974), GIP and its receptor (GIPR) are of high pharmacological interest, especially in identification and design of new molecules for the treatment of diabetes mellitus and obesity (Kieffer, 2003). The expression of GIPR in different organs and systems such as stomach, small intestine, adrenal cortex, pituitary, heart, testis, endothelial cells, bone, trachea, spleen, thymus, lung, kidney, thyroid and several regions of the CNS, increases the pharmacological importance of this receptor (Baggio and Drucker, 2007).

GIPR belongs to subfamily B1 of the G protein-coupled receptor (GPCR) superfamily, which also includes receptors for other hormones (Glucagon, GL; Glucagon-like peptide 1, GLP1; Glucagon-like peptide 2, GLP2; Secretin, SCT; Growth-hormone releasing hormone, GHRH; Vasoactive intestinal peptide, VIP; Pituitary adenylate cyclase-activating peptide, PACAP; Corticotrophin-releasing factor, CRF; Parathyroid hormone, PTH; Calcitonin, CT) (Gremlich et al., 1995; Volz et al., 1995). All receptors belonging to this family are composed of a large extracellular N-terminus that contains six highly conserved cysteine residues

forming three disulfide bridges, a serpentine domain with seven transmembrane helices, and a short intracellular C-terminus.

Receptor activation and subsequent intracellular signaling via Gαs protein closely follows the binding of GIP to GIPR (Baggio and Drucker, 2007; Volz et al., 1995). The recent structural characterization of the interaction between GIP and the extracellular domain (ectodomain, ECD) of its receptor demonstrates that GIPR interacts with the C-terminal two-third of GIP (1-30) peptide (Hinke et al., 2004; Parthier et al., 2007). GIP (1-30) activates GIPR, as demonstrated by intracellular production of cAMP, with equal potency as the *wild type* peptide GIP(1-42) (Gault et al., 2007; Hinke et al., 2003; Hinke et al., 2001). In contrast, fragment (7-30) of GIP showed a near maximal affinity with the receptor but had no detectable activity at micromolar concentration. However, fragment GIP(1-14) displayed a very low affinity but fully activated the GIPR at micromolar concentrations (Gault et al., 2007; Hinke et al., 2003; Hinke et al., 2001). All together, these data suggest that activation of GIPR by its natural ligand GIP involves high affinity binding of portion (7-30) of GIP to the N-terminal ECD of GIPR and activating interaction of N-terminal region (1-7) of GIP with the GIPR. However, there has been virtually no progress on the delineation of a ligand binding site for the N-terminal region of GIP (*i.e.* fragment 1-7) to its receptor so far. As a result, the precise mechanism whereby GIP activates its receptor remains unknown. Understanding ligand binding and receptor activation in GIPR has vital importance in the design of specific high affinity ligands with a desired pharmacological activity. With this in mind, and based on our experience with cholecystokinin and gastrin receptors (Dufresne et al., 2006), we have initiated this study aimed at the delineation of the binding site of human GIP receptor. Furthermore, given the fact that in family B of G-protein coupled receptors little is known about the region of the binding site formed by transmembrane helices, we focused our attention towards this domain of the GIP receptor. Using a strategy combining molecular

modeling and site-directed mutagenesis, we identified residues located in transmembrane

helices 2, 3, 5 and 6, which are important for GIP recognition by its receptor.

MATERIALS AND METHODS

Molecular Modeling of GIP receptor: The sequences of GIP receptors of different species were aligned against other members of subfamily B1 GPCRs to identify conserved hydrophobic regions estimated to be transmembrane helices. The initial model obtained from the multiple sequence alignment was further aligned against the sequence of bovine rhodopsin and A2a adenosine receptors, as the latter was chosen to be the structure template for the serpentine domain (Jaakola et al., 2008). All alignment investigations were done using ClustalX (Chenna et al., 2003). The final sequence alignment is in general agreement with the positioning of transmembrane helices provided by GPCR Data Base (Horn et al., 2003) (Figure 1).

The transmembrane helices of GIPR were constructed using side chain substitutions on the A2a adenosine receptor template (PDB ID: 3EML) (Jaakola et al., 2008). External and internal loops were added according to best fit and best homology using a protein template library in InsightII (InsightII). Special attention was paid to the structure generation of extracellular loop 2 (ECL2). Using a disulfide bridge constraint between Cys216 in transmembrane helix (TMH) 3 and Cys286 in ECL2, a structure was selected where ECL2 is located outside the transmembrane helix bundle leaving space to accommodate the GIP ligand. Similar to the A2a adenosine receptor template ECL2 in our model also participates in interactions with ECL1. After refinement of side chain interactions, the model was optimized by steepest descent energy minimization within MOE [Chemical Computing Group, Inc. (2008) Montreal, Quebec, Canada H3A 2R7].

For identification of receptor and ligand residues as potential interaction partners, sequences of subfamily B1 receptors of different species as well as sequences of corresponding ligands were aligned separately. Taking into account PTH, CRF, CT and their receptors, remaining ligands and receptors of subfamily B1 were focused in this identification

7

step, due to their closer sequence similarity (especially on ligand side). AnCoRe software package was used for identification of conserved residues as well as correlated mutations (Betancourt and Thirumalai, 1999; Murphy et al., 2000).

In manual docking investigations, the complex structure of GIP bound to the N-terminal ECD of GIPR (entry 2qkh, (Parthier, 2007 #7)) available in the PDB (Berman et al., 2000) has been used. Taking into account published experimental data on SCT and GL as well as potential interaction sites between peptides and receptors identified in multiple sequence alignment investigations, the complex of GIP-ECD was docked to GIPR. Resulting models, containing each GIP, GIPR ectodomain and GIPR transmembrane core, were optimized in side chain interaction and energy. Molecular dynamics simulations using Amber99 force field were applied in MOE for 1ns to check general reasonability of the formed complex structures.

Site-directed mutagenesis of GIPR and transient expression in HEK 293 cells: The plasmid containing the cDNA encoding human GIPR was kindly given by Professor Bernard Thorens (Lausanne, Switzerland). The sequence encoding the short variant of the GIPR was PCR amplified using a sense primer containing cloning site HindIII as well as sequence encoding Hemagglutinin epitope tag, YPYDVPDYA, and an antisense primer containing cloning site XhoI. PCR product was subcloned in pcDNA3 and sequenced. All mutants were constructed by oligonucleotide-directed PCR based mutagenesis using human GIPR cDNAs cloned in the pcDNA3 vector as a template. The presence of desired mutation and the absence of undesired mutation were confirmed by automated sequencing of the complete GIPR coding sequence. HEK 293 cells (2.5×10^6) were plated onto 10 cm culture dishes and grown in Dulbecco's Modified Eagle's Medium (DMEM) containing 10% fetal calf serum in a 5% CO_2 atmosphere at 37°C. After overnight incubation, cells were transfected with 12 μg/culture dish of pcDNA3 vector containing the cDNA for the wild-type or mutated GIP receptor, using

FUGENE 6 reagent in DMEM. The medium was aspirated 24 h later and was replaced with fresh medium with serum.

Cyclic Adenosine Mono Phosphate (cAMP) production by HEK 293 cells expressing GIP receptors (Horn et al.): Approximately 24 h after the addition of fresh DMEM and following overnight incubation, the transfected cells were rinsed with Dulbecco's Phosphate Buffered Saline (D-PBS). Cells were detached by scraping in the presence of 10 mL of D-PBS and incubated at 37 °C for 15 minutes with 0.25 mM 3-Isobutyl-1-methylxanthine (IBMX). Approximately 5 x 10^4 cells in a volume of 180 µL were stimulated by 20 µL of peptide (GIP (1-30) or Ala-substitued GIP(1-42)), in an increasing concentration from 10 pM to 10 µM, in duplicate tubes. To measure basal cAMP production, 180 µL of cells were added to 20 µL of D-PBS. All samples were incubated for 15 minutes at 37 °C. Reactions were stopped on ice and by addition of 800 µL of 95/5 of Methanol/Formic Acid. Tubes were capped, vortexed and left at -20°C overnight. The next morning all the samples and RIA cAMP kit (Immunotech, Marseille, France) were allowed to come to room temperature and the reagents were reconstituted. Samples or Calibrators were added to anti-cAMP antibody-coated tubes in the presence of 500 µL of ^{125}I-labelled cAMP tracer and incubated at 4°C for 18 h. Bound radioactivity was directly measured in a gamma counter (Auto-Gamma, Packard, Downers Grove, IL). Data were analyzed and graphs drawn up by using the non linear curve fitting software GraphPad Prism (San Diego, USA).

Synthesis and purification of GIP(1-30) amide: The Machine-assisted stepwise solid phase peptide synthesis (SPPS) was carried out on an Applied Biosystems model Pioneer™ Peptide Synthesis System using the standard procedures of Fmoc/tBu chemistry on a Tentagel S Ram resin from Rapp polymer and the crude peptide was obtained after a 2 h treatment with Trifluoroacetic acid/Triisopropylsilane/H_2O (95:2.5:2.5) followed by precipitation in a cold solution of methylbutylether/hexane (2/1). The compound was isolated by preparative HPLC

using a C8 column (5 mm, 250 x 21 mm) and mass-spectrometry [ESI-MS: m/z = 1767.0 $[M+2H]^{2+}$, 1178.2 $[M+3H]^{3+}$, 884.0 $[M+4H]^{4+}$; 3532.02 calculated for $C_{162}H_{240}N_{40}O_{47}S$]. Analytical HPLC confirmed peptide purity.

Preparation of GIP-Alexa-F 647: Coupling of GIP(1-30) to Alexa-F 647 was carried out by mixing at 20°C 20 nmol of GIP in solution in 0.1 M Sodium Borate, pH: 8.5 with 100 nmol of Alexa Fluor® carboxylic acid succinimidyl ester (Invitrogen, Carlsbad, Ca, USA) in solution in dimethyl formamid. After 6 h of reaction, the solution was submitted to HPLC separation on a nucleosil C18 column using a linear gradient of acetonitrile from 25% to 50% of acetonitrile in H_2O/ 0.05% Trifluoroacetic acid (Fig. 4).

Determination of expression levels of GIP receptors; HEK-293 cells (2 x 10^5) were cultured and transfected as described above. The cells were rinsed once with complete medium, detached in 1 mL of complete medium and transferred to special plastic tubes for flow cytometery analysis. The cells were rinsed by centrifugation at 1000 X rpm for 3 minutes at 4°C in the presence of 2-3 mL of 0.5% Bovine serum albumin-Phosphate buffer solution and then re-suspended in 100μL of incubation buffer. After an initial incubation for 10 minutes at room temperature, GIP-Alexa-F 647 was added with a final concentration of 10^{-7} M to the cells and incubated for 1 hour at room temperature in the dark. The cells were rinsed twice by centrifugation and re-suspended in 0.5 ml of incubation buffer and were analyzed by the flow cytometery (Becton Dickinson FACScalibur). The data was analyzed using Cell Quest Pro software both with reference to positive control i.e.; cells expressing wild type GIPR and negative control i.e.; non-transfected cells. For confocal microscopy visualization of GIPR expression, cells were grown on sterile 4-wells Lab-Teck coverglass chambers (Thermo Fisher Scientific, Roskilde, Denmark) coated with polylysine and incubated at 4°C for 2h with 1 μM GIP-Alexa-F 647 in D-PBS before observation using LSM 510 Zeiss confocal microscope (excitation at 633 nm by argon laser and emission > 650 nm).

10

MOL #60111

Background-subtracted images were assembled using Adobe Photoshop 7.0 (Adobe Systems,

Mountain View, CA).

11

RESULTS

Identification of putative binding site of GIP receptor by molecular modeling and in silico GIP docking: Based on multiple sequence alignments of both receptors and ligands, we constructed models of the GIPR-GIP complex using Adenosine A2a receptor as a template for the receptor's transmembrane helix bundle and taking X-ray structural data on the interaction of GIP and GIPR ECD into account (Parthier et al., 2007). Thereby, two binding modes showed reasonable interactions (Fig. 2).

In docking model A (Fig. 2a) GIP interacts with GIPR similar to a binding mode proposed for glucagon in glucagon receptor (Runge et al., 2003): the N-terminus of GIP is oriented in the direction of TMH1 of GIPR leaving residues Ala2 and Glu3 in-between TMH2 and TMH7, while GIP's helical structure lays on the receptor establishing contacts with ECL2 and ECL3. In this first model, Arg183 and Arg190 in TMH2 (Fig. 3) interact with Glu3 of GIP and Arg300 in TMH5 interacts with Asp15 of GIP. These interactions have been identified as important in this first binding mode and thus selected for mutation.

In docking model B (Fig. 2b) GIP interacts in GIPR similar to what has been described for the binding of secretin to secretin receptor (Dong et al., 2008): the N-terminus orients towards ECL3, allowing residues between it and the GIP's helical portion to find interactions within a binding grove made-up of TMH2, 3, 5, 6 and 7. Similar to binding mode A, binding mode B depends on interaction between Arg183 in TMH2 and Glu3 of GIP (Fig. 3). In contrast, Tyr1 and Ala2 of GIP established additional interactions within a typical GPCR ligand binding pocket. Residues Gln220, Thr223, Gln224 in TMH3, Arg300 in TMH5 and Phe357 in TMH6 have been predicted for experimental investigation to validate binding mode B. In addition and independently of the two described putative binding modes, we were interested in identifying residues with importance in receptor activation. Due to their close proximity to Arg183 (TMH2) and their possibility to establish a hydrogen bond network inside the

receptor, residues Asn230 (TMH3), Tyr231 (TMH3), His353 (TMH6) and Gln384 (TMH7) have been proposed for experimental investigation. The appearance of residues Asn230, Tyr231 and His353 in class B GPCRs seems to be related to Arg183 in TMH2. In contrast, Gln384 in TMH7 is one of the most conserved residues within all class B GPCRs and its corresponding residue in PTH/PTHrP receptors has been shown to be critical for ligand binding and receptor activation (Gardella et al., 1996).

We also proposed residue Tyr392 in TMH7 for investigation. This residue is not in close proximity to any putative residue of GIPR binding site. However, our sequence alignment investigations indicated that this residue corresponds to tyrosine in NPxxY motif, which has been demonstrated to be involved in activation of members of class A GPCRs (Gether, 2000).

Biological characterization of GIP-Alexa-F 647 and expression of GIPR mutants: Synthetic fragment 1-30 of GIP was coupled to Alexa Fluor® succinimidyl ester and the coupling medium was submitted to reverse phase HPLC. According to mass spectrometry analysis of trypsin digested fragments and N-terminal amino acid determination (data not shown), compound contained in the major peak eluted at 16.5 min. corresponded to GIP coupled to Alexa Fluor® through Lys30 (Fig. 4a). GIP-Alexa-F 647 thus purified stimulated cAMP formation in HEK-293 cells expressing the GIPR with potency and efficacy similar to GIP(1-30) (Fig. 4b). GIP-Alexa-F 647 was further used for measurement of GIPR mutant expression at the cell surface which might be affected by site-directed mutagenesis substitution of residues in the GIPR. In the first series of experiments, batches of cells expressing the different mutants were incubated with GIP-Alexa-F 647 at a saturating concentration (1 μM) and analyzed by flow cytometry. Values from fluorescence-activated cell sorting profiles indicated that all mutants were expressed at HEK-293 cell membrane at levels similar that of the wild-type GIPR (table). In a second series of experiments, cells plated on microscope lab-teck coverglass chambers were incubated on ice with GIP-Alexa-F

647 (1 μM) and observed by confocal microscopy. Photographs shown on figure 5 demonstrated that all mutants were expressed at the HEK-293 cell surface and at comparable levels to that of the wild-type GIPR.

Pharmacological and site-directed mutagenesis identification of amino acids involved in GIP-induced cAMP production: We further aimed to pharmacologically test our proposed models for binding of GIP to GIPR. Main residues identified in these different 3D models, namely Arg183, Arg190, Gln220, Thr223, Gln224, Asn230, Tyr231, Arg300, His353, Phe357, Gln384 and Tyr392 were each exchanged for an alanine and, additionally, Gln384 for an asparagine and Tyr231 for a phenylalanine. Performing activity assays on HEK-293 cells expressing these mutants allowed identifying positions important in ligand-induced receptor activation by shifts in potency of measured cAMP-production (Fig.6 and table).

The biggest influence of alanine substitution on GIP potency was discovered for Arg183Ala (F_{mut} 76.4, $p<0.001$) and Arg190Ala (F_{mut} 71.2, $p<0.001$), both located in TMH2. Important decreases in potency were also found for Arg300Ala in TMH5 (F_{mut} 42.0) and Phe357Ala in TMH6 (F_{mut} 15.7). Furthermore, significant decreases ($p<0.001$) were observed for Gln220Ala, Thr223Ala, Gln224Ala and Asn230Ala, all in TMH3 (table). In contrast, minor influence has been noticed for Tyr231 (TMH3), His353 (TMH6), Gln384 (TMH7) and Tyr392 (TMH7). Efficacy (maximum cAMP production) by which all mutants responded to GIP was close to that of the wild-type receptor (table 1).

Pharmacological discrimination between the theoretical models A and B of GIPR-GIP complex: To discriminate between the two theoretical docking models for GIPR-GIP complexes, we aimed at identification of interacting charged amino acid in both the GIPR and GIP as we previously carried out with cholecystokinin receptors (Gigoux et al., 1999; Silvente-Poirot et al., 1999). A pharmacological support for the interactions was first based on

the assumption that mutation of putative interacting amino acids in GIP and in GIPR should cause equivalent shifts in potency in cAMP production. To further assess the interaction, we reasoned that mutating simultaneously the interacting amino acids in GIP and GIPR should not further shift the potency in cAMP production relative to single mutation on either GIP or GIPR. On the contrary, simultaneous exchange of residues that does not interact should induce an additional decrease in the potency relative to single mutation on either GIP or GIPR.

In the two models A and B of GIPR-GIP complex, Arg183 in TMH2 (Fig. 3a) interact with Glu3 of GIP. On the other hand, Arg183 and Arg190 are only two helix turns distant from each other, which is comparable to the distance of Glu3 and Asp9 in GIP thus suggesting that Arg190 interacts with Asp9. Therefore, we first determined the influence of Glu3Ala and Asp9Ala substitution in GIP. As illustrated in Fig. 7, potency of GIP to stimulate Arg183Ala GIPR was identical to potency of Ala3GIP to stimulate the wild-type GIPR. In addition, no further significant decrease in potency was seen when Ala3GIP was used to stimulate Arg183Ala GIPR. This strongly supports that Arg183 directly and uniquely interacts with Glu3 of GIP to induce cAMP formation. In contrast, Ala9-GIP at concentration up to 10 μM did not stimulated cAMP production through R183A-GIPR suggesting no direct interaction between Arg183 and Asp9 of GIP.

As for Arg190, experiments shown in Fig. 8 indicate that Glu3Ala substitution in GIP and Arg190Ala substitution in GIPR result in equal decrease in potency. However, simultaneous mutations in ligand and receptor produced an additional dramatic shift in potency relative to the single alanine substitutions ($EC_{50} > 10$ μM versus 0.1 μM), as well as a dramatic decrease in cAMP production level. On the other hand, potency of GIP to stimulate Arg190Ala-GIPR was very close to the potency of Ala9GIP to stimulate wild-type GIPR but Ala9GIP did not stimulate Arg190Ala-GIPR. All together, these data allow us to conclude that direct

15

interactions taking place between Arg190 in GIPR and Glu3 in GIP as well as between Arg190 in GIPR and Asp9 of GIP are very unlikely.

One major difference between the two theoretical binding modes A and B concerns Arg300 in the GIPR which interacts with Asp15 of GIP in model A while it interacts with Tyr1 of GIP in model B. Furthermore, another important difference concerns Tyr-Ala sequence of GIP, which lays on GIPR surface in model A while it interacts more deeply in the binding pocket with Phe357, Arg300, Gln220, Thr223 and Gln224 in model B of docking.

It is also worth specifying that in model A, Glu3 is in close proximity to Arg300 and Phe357. However, charge interactions between Arg300 and Glu3 of GIP were not recognized, due to Phe357 benzene ring interfering between both charged residues.

We therefore first analyzed experimentally possible interactions between Arg300 and Glu3 of GIP as well as with other negatively charged residues in GIP, namely Asp9 and Asp15. Results from these experiments are shown on Fig. 9. Alanine substitution of Glu3, Asp9 or Asp15 caused 28, 35 and 20-fold decreases in the potency of GIP to stimulate the wild-type GIP receptor, respectively (experiments shown in Fig. 7, 8, 9). Substitution Arg300Ala in the GIPR decreased by 42–fold the potency by which the receptor responded to GIP (table 2, Fig. 6). Double mutations in both GIP at position 3, 9 or 15 and in GIPR at position Arg300 caused further dramatic shifts in cAMP production potency relative to single substitution either on the peptide or on the receptor, supporting that none of the three acidic amino acids of GIP (Glu3, Asp9 and Asp15) interacts with Arg300. As a result, docking mode A is not supported by experimental data concerning Arg300Ala. In contrast, decrease in potency found for Arg300Ala and Phe357Ala mutants (F_{mut} 42.0 and 15.7, respectively) together with those observed with Gln220Ala, Thr223Ala, Gln224Ala and Asn230Ala mutants all in TMH3 (F_{mut} 4.7, 3.4, 5.6 and 6.5, respectively, table 2), clearly support the model of GIP.GIPR complex corresponding to docking mode B.

Finally, since in the PTH2 receptor, residue equivalent to Arg183 in GIPR was shown to be functionally linked to reside equivalent to Gln384 in GIPR (Gardella et al., 1996), we double- mutated GIPR at the two positions 183 and 384. Double mutation Arg183Ala.Gln384Ala decreased the efficacy (75%) and the potency (14-fold) by which the GIPR responded to GIP to stimulate cAMP production (Fig. 10). Interestingly, shift of potency caused by the double mutation was smaller than that caused by the single mutation Arg183Ala (16.6 fold versus 76.4-fold, fig. 10). Expression experiments indicated that the double mutant was significantly less expressed at the cell surface than the wild-type GIP (12 % of wild-type GIPR expression, not shown) suggesting that the apparent decreased in cAMP production was solely caused by the drop in expression of the double-mutant.

Description of the binding pocket in GIP receptor involved in interaction with N-terminal moiety of GIP for identified binding mode B: In binding mode B (Fig. 11), which is strongly supported by pharmacological data, GIP rests, with its C-terminus bound to the ECD, in a binding grove between ECL2 and ECL3. This way, residues of GIP's N-terminal portion (residues 1 to 5) find interactions within the transmembrane helix bundle.

In detail, Tyr1 of GIP establishes a hydrogen bond to Gln224 (TMH3) and π-cation interaction to the guanidino group of Arg300 (TMH5). In addition, Tyr1 rests in a hydrophobic pocket consisting of Ile295 (TMH5), Val360 (TMH6) and Phe357 (TMH6). These interactions are in agreement with the shifts in potency for cAMP production resulting from alanine substitution these residues in GIPR: Gln224 (5.6-fold), Arg300 (42-fold) and Phe357 (15.7-fold). The methyl side chain of Ala2 in GIP finds a corresponding environment in TMH3 close to Gln220 and Thr223. Glu3 of GIP interacts with Arg183 (TMH2). The interaction is based on charge polarized hydrogen bonds. We also recognized the possibility of hydrogen bonding between Glu3 backbone NH with the side chain carbonyl of Gln220 (TMH3) during MD simulation (interaction not shown). Residue Gly4 of GIP is not involved

17

in direct receptor ligand interactions but its small size allows a close orientation to TMH1 in the narrow space between TMH2 and TMH7.

We further suggest the necessity of the formation of a turn-like structure in GIP's N-terminus while interacting in GIPR: Ala2 backbone carbonyl oxygen is involved in hydrogen bonding to the backbone NH of Thr5 of GIP, which in return caps the N-terminus of GIP central helix moiety via its side chain In addition, the flexible character of Gly4 supports the formation of a turn-like, which fits into the narrow space between TMHs 1, 2, and 7.

Concerning residues Asp9 and Asp15 of GIP which, in the current study, have not been found to pair with amino acids of TMH in the GIPR, model B of GIPR-GIP complex shows the following interactions: Asp9 interacts with Asn283 and Arg289 in ECL2, two residues being each 3 amino acids apart the central and conserved cystein residue (Cys286); Asp15 is involved in interactions with the N-terminus of the ECD and intramolecularly with Gln19 in GIP, a result which corresponds to what has been found in the X-ray structure (Parthier et al., 2007).

DISCUSSION

Owing to the high importance of members of group B of the GPCR family in physiology, the understanding of the mechanism by which they are activated by their natural ligands, as well as the discovery of non peptide ligands for those receptors represent timely challenges. Identification of ligand binding sites represents a key step which should greatly help to take up these challenges. In the current study, our aim was to gain insight into the binding site of human GIPR, with a special focus on residues that were expected to interact with the N-terminal portion of GIP. According to structure-activity relationship data and the recent crystal structure of the complex formed between GIPR ECD and GIP, these residues are the most fundamental for receptor activation, while not being involved in high affinity and selectivity binding with GIPR ECD (Parthier et al., 2007). Based on our past and successful experience with cholecystokinin and gastrin receptors, we used in synergy molecular modeling to propose candidates in both receptor and ligand and applied site-directed mutagenesis to pharmacologically evaluate theoretical predictions (Gigoux et al., 1999; Silvente-Poirot et al., 1999). For pharmacological characterization of the interactions, we analysed the impact of receptor mutations on cAMP production rather than on binding of radio-iodinated GIP because we aimed at identifying amino acids involved in ligand-dependent receptor activation and because there exist discrepancies between contribution to affinity and to activity of amino acids analyzed (Gault et al., 2007; Hinke et al., 2001). Moreover, radio-iodination of GIP requires modification of Tyr1, a critical residue which is likely to be directly involved in GIPR activation.

GIP was initially docked in our GIPR models orienting its N-terminus in different potential binding modes based on information on GPCR binding sites as well as on photo-labeling investigations of secretin and glucagon in their corresponding receptors (Dong et al., 2008; Runge et al., 2003). Taking into account experimental data on other class B GPCRs as

well as the recently identified interaction of GIP in the GIPR ECD, an orientation of the N-terminal portion of GIP between TMH2 and TMH3 as well as TMH6 and TMH7 has been selected as most suitable. Pharmacological analysis of GIPR mutants are moreover in favor of the binding site for GIP's N-terminus in which Glu3 in GIP is in functional interaction with Arg183 and biologically crucial Tyr1 interacts with Gln224 (TMH3), Arg300 (TMH5) and Phe357 (TMH6). From our knowledge, such precise structural information on this area of the GIPR binding site was not available yet. Theoretical data from a modeling study has been reported earlier (Malde et al., 2007), but corresponding study lacks experimental validation and is not in agreement with our results from experiments.

Interaction of Arg183 in GIPR with Glu3 in GIP appears crucial for agonist-induced receptor activation. Of interest, this receptor residue is conserved within all members of subfamily B1 and there is now a general agreement for its interaction with the amino acid located in position 3 in the cognate ligands. For example, in the rat secretin receptor, substitution of Arg166 equivalent to Arg183 in the GIPR also dramatically decreased potency of secretin to stimulate cAMP production, and this residue was shown to interact with Asp3 of secretin. In the VPAC1 and VPAC2 receptors, the mutation of the corresponding basic amino acids was reported to affect potency of VIP to stimulate the receptors (Solano et al., 2001; Vertongen et al., 2001). As for rat secretin receptor, pharmacological analysis of the mutants using substituted peptide analogues provided evidence that Asp3 in VIP was likely interacting with basic amino acid equivalent to Arg183 in the GIPR. In the PTH1and PTH2 receptors Arg233 and Arg190 equivalent to Arg183 in the GIPR were also shown to be critical for high affinity binding of PTH and high potency activation of the receptors (Gardella et al., 1996; Turner et al., 1998).

On the contrary to Arg183, Arg190 in GIPR was not found to interact directly with an acidic residue of the ligand, although it is also critical for potency by which GIP induces

cAMP. Equivalent residues to Arg190 were reported to be important in other members of group B1 GPCRs and were proposed to act as a selectivity filter in ligand recognition for GL-, SCT-, and VIP-R (Di Paolo et al., 1998; Perret et al., 2002; Waelbroeck et al., 2002). Indeed, a negative charge is conserved in position 3 of ligand peptides GIP, SCT, VIP, PACAP, GHRH, GLP1, and GLP2 but not in GL The corresponding receptors of these peptides but not GL-R share two positive charges in the corresponding positions to Arg190 and Arg183 in GIPR. In contrast, in GL-R only Lys187, the positive charge corresponding to GIPR's Arg183, in TMH2 is conserved,, whereas the corresponding amino acid to GIPR's Arg190 is the uncharged residue isoleucine. Therefore, there exists a correlation between absence of 2nd positive charge in TMH2 of GL-R (in comparison to other class B GPCRs) and presence of the uncharged Gln3 in GL supporting that the basic residue corresponding to Arg190 in the GIPR may play a role of selective filter in group B1 GPCRs.

In the PTH2 receptor, Arg233 equivalent to Arg183 in GIPR was shown to be functionally linked to a conserved reside of helix VII, namely Gln451 (Gardella et al., 1996). In the PTH2 receptor, exchange of Gln451 for a Lys reduced the binding affinity of PTH and when this mutation was combined with that of Arg233 in helix II, binding affinity of the double mutant for PTH was almost restored but no more cAMP production could be detected (Gardella et al., 1996). Although in the case of GIPR, a different situation seems to occur, our modeling and experimental results with GIPR also strongly support spatial proximity and functional link between conserved Arg of helix II and Gln of helix VII. In the current study, we show that the alanine exchange of the conserved Gln of helix VII, namely Gln384, decreased potency with which GIP stimulates its receptor by 2.6-fold (table). Introducing a double mutation of Arg183 and Gln384 in GIPR caused a smaller shift in potency than single mutation of Arg183 but dramatically decreased apparent efficacy with which the GIPR

responded to GIP, a result which may be due to the drop of expression of double-mutant as a functional receptor at the cell surface.

Another important new finding provided by the current study concerns residues in functional interaction with Tyr1 of GIP which were found located in three different TMH of the GIPR. These are Arg300 (TMH5), Phe357 (TMH6) and Gln224 (TMH3) which appear, in the model, to bind GIP Tyr1 through π-cation interaction, hydrophobic contacts and a hydrogen bond, respectively. Although sequence alignment investigations of subfamily B1 GPCRs indicates a high degree of conservation of these three amino acids in class B of GPCRs, analysis of the cognate ligands shows the presence of a Tyrosine at position 1 only in GIP and GRF whereas other ligands have an histidine at this position. It is likely that, due to differences in physico-chemical properties, Tyr1 of GIP involves a unique network of interactions in GIPR. This may explain why mutation of Arg277 in rat SCT receptor corresponding to Arg300 in GIPR does not affect SCT-induced cAMP production (Di Paolo et al., 1999).

Our data on GIP-GIPR interaction shows another particularity: the formation of a turn-like structure made-up by residues Ala2-Glu3-Gly4-Thr5. We think that a turn-like conformation of GIP's N-terminus is supported by the small but significant effects on ligand induced receptor activation in Gln220- and Thr223-mutants. Gln220- and Thr223 in TMH3 provide a favorable environment for a turn-like structure of GIP. This observation is in agreement with the idea that the N-termini of class B1 receptor peptide ligands have to adopt a specific conformation to finally activate their receptor (Neumann et al., 2008). This hypothesis, together with the finding that Arg183 in GIPR interacts with Glu3 in GIP, allows us to propose a possible explanation, why the substitution of Glu3 to proline in GIP results in an antagonistic ligand for GIPR (Gault et al., 2002). Indeed, we suggest that this substitution favors the formation of a turn-like structure established by residues Ala2-Pro3-Gly4-Thr5

which subsequently finds good interactions within the GIPR binding pocket while maintaining the receptor in an inactive state (Fig. 12).

So far, and unlike for members of group A of GPCR, mechanism by which members of group B are activated by their cognate ligands remains poorly documented. Structurally, these receptors lack conserved motifs and residues such as E/DRY, NPXXY motifs which have been involved in the activation process of group A GPCRs. However, a general mechanism of peptide ligand interaction with class B GPCRs has emerged, termed the 'two-domain' model in which the C-terminal moiety of the ligand binds with a high affinity and selectivity to receptor ECD within a period of time less than 140 ms followed by slower binding of ligand N-terminal to TMH of the receptor to activate it and triggers G protein coupling (Castro et al., 2005). The precise underlying mechanisms corresponding to this second step remains to be elucidated. However, it is plausible to consider that part of the binding site formed by the TMH core could be targeted by appropriate non peptide ligands as has been possible for most class A GPCRs, and therefore will be amenable to medicinal chemistry. Future works will be dedicated to the refinement of the modeled structure of this region of the GIP binding site in GIPR and to the understanding of the activation mechanism in GIPR.

REFERENCES:

Baggio LL and Drucker DJ (2007) Biology of incretins: GLP-1 and GIP. *Gastroenterology* **132**(6):2131-2157.

Ballesteros JA and Weinstein H (1995) Integrated methods for the construction of three dimensional models and computational probing of structure-function relations in G-protein coupled receptors. *Methods Neurosci* **25**:366-428.

Berman HM, Westbrook J, Feng Z, Gilliland G, Bhat TN, Weissig H, Shindyalov IN and Bourne PE (2000) The Protein Data Bank. *Nucleic Acids Res* **28**(1):235-242.

Betancourt MR and Thirumalai D (1999) Pair potentials for protein folding: choice of reference states and sensitivity of predicted native states to variations in the interaction schemes. *Protein Sci* **8**(2):361-369.

Brown JC (1974) Candidate hormones of the gut. 3. Gastric inhibitory polypeptide (GIP). *Gastroenterology* **67**(4):733-734.

Castro M, Nikolaev VO, Palm D, Lohse MJ and Vilardaga JP (2005) Turn-on switch in parathyroid hormone receptor by a two-step parathyroid hormone binding mechanism. *Proc Natl Acad Sci U S A* **102**(44):16084-16089.

Chenna R, Sugawara H, Koike T, Lopez R, Gibson TJ, Higgins DG and Thompson JD (2003) Multiple sequence alignment with the Clustal series of programs. *Nucleic Acids Res* **31**(13):3497-3500.

Di Paolo E, De Neef P, Moguilevsky N, Petry H, Bollen A, Waelbroeck M and Robberecht P (1998) Contribution of the second transmembrane helix of the secretin receptor to the positioning of secretin. *FEBS Lett* **424**(3):207-210.

Di Paolo E, Vilardaga JP, Petry H, Moguilevsky N, Bollen A, Robberecht P and Waelbroeck M (1999) Role of charged amino acids conserved in the vasoactive intestinal polypeptide/secretin family of receptors on the secretin receptor functionality. *Peptides* **20**(10):1187-1193.

Dong M, Gao F, Pinon DI and Miller LJ (2008) Insights into the Structural Basis of Endogenous Agonist Activation of Family B G Protein-Coupled Receptors. *Mol Endocrinol*.

Dufresne M, Seva C and Fourmy D (2006) Cholecystokinin and gastrin receptors. *Physiol Rev* **86**(3):805-847.

Gardella TJ, Luck MD, Fan MH and Lee C (1996) Transmembrane residues of the parathyroid hormone (PTH)/PTH-related peptide receptor that specifically affect binding and signaling by agonist ligands. *J Biol Chem* **271**(22):12820-12825.

Gault VA, Hunter K, Irwin N, Green BD, Greer B, Harriott P, O'Harte FP and Flatt PR (2007) Characterisation and biological activity of Glu3 amino acid substituted GIP receptor antagonists. *Arch Biochem Biophys* **461**(2):263-274.

Gault VA, O'Harte FP, Harriott P and Flatt PR (2002) Characterization of the cellular and metabolic effects of a novel enzyme-resistant antagonist of glucose-dependent insulinotropic polypeptide. *Biochem Biophys Res Commun* **290**(5):1420-1426.

Gether U (2000) Uncovering molecular mechanisms involved in activation of G protein-coupled receptors. *Endocr Rev* **21**(1):90-113.

Gigoux V, Escrieut C, Fehrentz JA, Poirot S, Maigret B, Moroder L, Gully D, Martinez J, Vaysse N and Fourmy D (1999) Arginine 336 and asparagine 333 of the human cholecystokinin-A receptor binding site interact with the penultimate aspartic acid and the C-terminal amide of cholecystokinin. *J Biol Chem* **274**(29):20457-20464.

Gremlich S, Porret A, Hani EH, Cherif D, Vionnet N, Froguel P and Thorens B (1995) Cloning, functional expression, and chromosomal localization of the human pancreatic islet glucose-dependent insulinotropic polypeptide receptor. *Diabetes* **44**(10):1202-1208.

Hinke SA, Gelling R, Manhart S, Lynn F, Pederson RA, Kuhn-Wache K, Rosche F, Demuth HU, Coy D and McIntosh CH (2003) Structure-activity relationships of glucose-dependent insulinotropic polypeptide (GIP). *Biol Chem* **384**(3):403-407.

Hinke SA, Manhart S, Pamir N, Demuth H, R WG, Pederson RA and McIntosh CH (2001) Identification of a bioactive domain in the amino-terminus of glucose-dependent insulinotropic polypeptide (GIP). *Biochim Biophys Acta* **1547**(1):143-155.

Hinke SA, Manhart S, Speck M, Pederson RA, Demuth HU and McIntosh CH (2004) In depth analysis of the N-terminal bioactive domain of gastric inhibitory polypeptide. *Life Sci* **75**(15):1857-1870.

Horn F, Bettler E, Oliveira L, Campagne F, Cohen FE and Vriend G (2003) GPCRDB information system for G protein-coupled receptors. *Nucleic Acids Res* **31**(1):294-297.

Jaakola VP, Griffith MT, Hanson MA, Cherezov V, Chien EY, Lane JR, Ijzerman AP and Stevens RC (2008) The 2.6 angstrom crystal structure of a human A2A adenosine receptor bound to an antagonist. *Science* **322**(5905):1211-1217.

Jornvall H, Carlquist M, Kwauk S, Otte SC, McIntosh CH, Brown JC and Mutt V (1981) Amino acid sequence and heterogeneity of gastric inhibitory polypeptide (GIP). *FEBS Lett* **123**(2):205-210.

Kieffer TJ (2003) GIP or not GIP? That is the question. *Trends Pharmacol Sci* **24**(3):110-112.

Malde AK, Srivastava SS and Coutinho EC (2007) Understanding interactions of gastric inhibitory polypeptide (GIP) with its G-protein coupled receptor through NMR and molecular modeling. *J Pept Sci* **13**(5):287-300.

Mentlein R, Gallwitz B and Schmidt WE (1993) Dipeptidyl-peptidase IV hydrolyses gastric inhibitory polypeptide, glucagon-like peptide-1(7-36)amide, peptide histidine methionine and is responsible for their degradation in human serum. *Eur J Biochem* **214**(3):829-835.

Moody AJ, Thim L and Valverde I (1984) The isolation and sequencing of human gastric inhibitory peptide (GIP). *FEBS Lett* **172**(2):142-148.

Murphy LR, Wallqvist A and Levy RM (2000) Simplified amino acid alphabets for protein fold recognition and implications for folding. *Protein Eng* **13**(3):149-152.

Neumann JM, Couvineau A, Murail S, Lacapere JJ, Jamin N and Laburthe M (2008) Class-B GPCR activation: is ligand helix-capping the key? *Trends Biochem Sci* **33**(7):314-319.

Parthier C, Kleinschmidt M, Neumann P, Rudolph R, Manhart S, Schlenzig D, Fanghanel J, Rahfeld JU, Demuth HU and Stubbs MT (2007) Crystal structure of the incretin-bound extracellular domain of a G protein-coupled receptor. *Proc Natl Acad Sci U S A* **104**(35):13942-13947.

Perret J, Van Craenenbroeck M, Langer I, Vertongen P, Gregoire F, Robberecht P and Waelbroeck M (2002) Mutational analysis of the glucagon receptor: similarities with the vasoactive intestinal peptide (VIP)/pituitary adenylate cyclase-activating peptide (PACAP)/secretin receptors for recognition of the ligand's third residue. *Biochem J* **362**(Pt 2):389-394.

Runge S, Wulff BS, Madsen K, Brauner-Osborne H and Knudsen LB (2003) Different domains of the glucagon and glucagon-like peptide-1 receptors provide the critical determinants of ligand selectivity. *Br J Pharmacol* **138**(5):787-794.

Silvente-Poirot S, Escrieut C, Gales C, Fehrentz JA, Escherich A, Wank SA, Martinez J, Moroder L, Maigret B, Bouisson M, Vaysse N and Fourmy D (1999) Evidence for a direct interaction between the penultimate aspartic acid of cholecystokinin and histidine 207, located in the second extracellular loop of the cholecystokinin B receptor. *J Biol Chem* **274**(33):23191-23197.

Solano RM, Langer I, Perret J, Vertongen P, Juarranz MG, Robberecht P and Waelbroeck M (2001) Two basic residues of the h-VPAC1 receptor second transmembrane helix are essential for ligand binding and signal transduction. *J Biol Chem* **276**(2):1084-1088.

Turner PR, Mefford S, Bambino T and Nissenson RA (1998) Transmembrane residues together with the amino terminus limit the response of the parathyroid hormone (PTH) 2 receptor to PTH-related peptide. *J Biol Chem* **273**(7):3830-3837.

Vertongen P, Solano RM, Perret J, Langer I, Robberecht P and Waelbroeck M (2001) Mutational analysis of the human vasoactive intestinal peptide receptor subtype VPAC(2): role of basic residues in the second transmembrane helix. *Br J Pharmacol* **133**(8):1249-1254.

Volz A, Goke R, Lankat-Buttgereit B, Fehmann HC, Bode HP and Goke B (1995) Molecular cloning, functional expression, and signal transduction of the GIPReceptor cloned from a human insulinoma. *FEBS Lett* **373**(1):23-29.

Waelbroeck M, Perret J, Vertongen P, Van Craenenbroeck M and Robberecht P (2002) Identification of secretin, vasoactive intestinal peptide and glucagon binding sites: from chimaeric receptors to point mutations. *Biochem Soc Trans* **30**(4):437-441.

MOL #60111

FOOTNOTES

e) Address for reprint request: Daniel Fourmy, U858 INSERM I2MR, equipe 13, 1 avenue Jean Poulhès, BP 84225, 31432 Toulouse Cedex 4, France; Phone: (33) 5 61 32 30 57, fax: (33) 6 61 32 24 03 . Email: Daniel.Fourmy@inserm.fr

27

LEGENDS TO FIGURES:

Fig. 1: Sequence alignment of transmembrane helices for GIP receptor, adenosineA2a-R and bovine rhodopsin. Ballesteros and Weinstein's GPCR residue indexing is shown (Ballesteros and Weinstein, 1995).

Fig. 2: Schematic representation of theoretical docking modes of GIP to the GIP receptor. Molecular docking investigations resulted in two different potential binding modes of GIP in GIPR. The binding modes resemble the differently described receptor ligand interactions for homologous class B GPCRs GL-R and SCT-R. Although the complex of GIP and GIPR ECD shows different orientations regarding the transmembrane helix bundle, both models showed reasonable contact sites.

Fig. 3: Primary structure of GIP and serpentine representation of GIP receptor. In the upper part of the figure, aminoacid sequence of GIP is given. In the serpentine representation of the human GIPR, residues which have been mutated (circled letters), extracellular domain (ECD), extracellular loops (ECL1, ECL2, ECL3) and transmembrane helices (TMHI-VII) are depicted.

Fig. 4: Preparation and biological activity of GIP-Alexa-F 647. A: High performance liquid chromatography purification of GIP-Alexa-F 647. The separation was performed as described in the "Methods" section. Absorption pic 9 (280 nm) eluted at 16.0 min. corresponded to GIP coupled to Alexa-F 647 through Lys30. B: Biological activity of GIP-Alexa-F 647. GIP- or GIP-Alexa-F 647-induced cAMP production was measured in HEK-293 cells expressing the human GIP receptor. Results are expressed as percent of maximum cAMP production in the presence of GIP. EC50 were 2.9 nM and 5.7 nM for GIP and for GIP-Alexa-F 647, respectively (n=2).

Fig. 5: Expression of GIP receptors in HEK 293 cells. For quantification of expression and visualization of wild-type and mutated GIPR, transfected cells were incubated with 0.1-1

μM GIP-Alexa-F 647 and analyzed by flow cytometry or observed by confocal microscopy as described in the methods section. Representative microscopy pictures are shown for only 6 GIPR variants but expression of all GIPR mutants at the cell surface of HEK-293 cells was visualized.

Fig. 6: Importance of residues Arg183, Arg190, Phe357 and Arg300 in the GIP receptor for GIP-induced cAMP production. Wild-type GIP receptor or mutants R183A, R190A, F357A or R300A were expressed in HEK 293 cells and stimulated for 15 min by GIP for cAMP production measurement.

Mutation factors (Fwt) were calculated as EC_{50} (mutated GIPR)/EC_{50} (WT-GIPR). Emax values are expressed as percent of wild-type receptor maximal cAMP production in response to 1 μM GIP. Cell surface expression of the mutants of the GIPR was assessed by flow cytometry using GIP-Alexa-F 647 as ligand and was expressed as percent of the value achieved with wild-type GIPR. Results represent the means ± SEM of at least four independent experiments performed in duplicate on separately transfected HEK-293 cells. Calculated EC_{50} are reported in table 1.

Fig. 7: Pharmacological evidence for a direct interaction between of Arg183 of GIPR and Glu3 of GIP but not Asp9. Wild-type GIP receptor or mutant R183A-GIPR were expressed in HEK-293 and stimulated for 15 min either by GIP, Ala3-GIP or Ala9-GIP for cAMP production measurement. In these series of experiments, calculated potencies (EC_{50}, nM) were: WT-GIPR.GIP: 3.7 nM, WT-GIPR.Ala3-GIP: 103 nM, R183A-GIPR.GIP: 109 nM; R183A-GIPR.Ala3-GIP: 128 nM; WT-GIPR.Ala9-GIP: 131 nM; R183A-GIPR.Ala9-GIP> 10^4 nM. Values for cAMP production are expressed as percent of maximum cAMP production obtained with the wild-type GIPR stimulated by GIP. Results represent the means of at least three independent experiments performed in duplicate on separately transfected HEK-293 cells.

Fig. 8: Pharmacological evidence that Arg190 in GIP receptor does not interact with Glu3 or Asp9 of GIP. Wild-type GIP receptor or mutants R190A-GIPR were expressed in HEK-293 and stimulated for 15 min either by GIP, Ala3-GIP or Ala9-GIP for cAMP production measurement. Calculated potencies (EC_{50}, nM) were: WT-GIPR.GIP: 2.4 nM, WT-GIPR.Ala3-GIP: 103 nM, WT-GIPR.Ala9-GIP: 120 nM, R190A-GIPR.GIP: 104 nM; R190A-GIPR.Ala3-GIP: $> 10^4$ nM; R190A-GIPR.Ala9-GIP: $>10^4$ nM. Values for cAMP production are expressed as percent of maximum cAMP production obtained with the wild-type GIPR stimulated by GIP. Results represent the means of at least three independent experiments performed in duplicate on separately transfected HEK-293 cells.

Fig. 9: Pharmacological evidence that Arg300 in GIP receptor does not interact with Glu3, Asp9 or Asp15 of GIP. HEK-293 cells expressing the wild-type GIP receptor or mutants R300A-GIPR were expressed in HEK-293 and stimulated for 15 min either by GIP, Ala3-GIP, Ala9-GIP or Ala15-GIP for cAMP production measurement. Calculated potencies (EC_{50}, nM) were: WT-GIPR.GIP: 3.0 nM; WT-GIPR.Ala15-GIP: 63 nM; R300A-GIPR.GIP: 87 nM; R300A-GIPR.Ala3-GIP: $> 10^4$ nM; R300A-GIPR.Ala9-GIP: $> 10^4$ nM; R300A-GIPR.Ala15-GIP: $> 10^4$ nM. Values for cAMP production are expressed as percent of maximum cAMP production obtained with the wild-type GIPR stimulated by GIP. Results represent the means of at least three independent experiments performed in duplicate on separately transfected HEK-293 cells.

Fig. 10: Effects of single mutation Gln384Ala and double mutation Arg183Ala.Gln384Ala on GIP-induced cAMP production. HEK-293 cells expressing the wild-type GIP receptor or mutants were expressed in HEK-293 and stimulated for 15 min by GIP for cAMP production measurement. Calculated potencies (EC_{50}, nM) were: WT-GIPR: 1.96 ± 0.32 nM; Gln384Ala-GIPR: 5.2 ± 1.4 nM; Arg183Ala.Gln384Ala-GIPR: 32.5 ± 12.3 nM. Values for cAMP production are expressed as percent of maximum cAMP production

obtained with the wild-type GIPR stimulated by GIP. Results represent the means of at least three independent experiments performed in duplicate on separately transfected HEK-293 cells. It is worthy to note that expression level of double mutant was only 12 % of that of WT-GIPR.

Fig. 11: Model of the interactions of GIP N-terminus in the binding pocket of GIPR. The ligand receptor interaction follows binding mode B, which has been identified as most suitable to explain our experimental data. Important GIPR residues in ligand binding are shown in atom colors with cyan carbons. Residues of GIP's N-terminus involved in these interactions are shown in atom colors with green carbons. Hydrogen bond contacts, which remained stable during MD simulation, are shown as magenta lines. Tyr1 of GIP establishes a hydrogen bond to Gln224 (TMH3) and π-cation interaction to the guanidino group of Arg300 (TMH5). It also rests in a hydrophobic pocket containing Phe357 (TMH6) as main contributor. GIP's Glu3 interacts with Arg183 (TMH2). Hydrogen bonding between Glu3's backbone NH with the side chain carbonyl of Gln220 (TMH3) is possible (not shown). The small side chain of GIP's Gly4 allows a close orientation to TMH1 in the narrow space between TMH2 and TMH7.

Figure 12: Comparison between models of N-terminus docking of GIP and its antagonistic derivative Glu3Pro-GIP in the GIPR binding site. Ligand and receptor orientation and representation follow the style in Figure 11. Pro3 inGlu3Pro-GIP supports the formation of the turn-like structure we suggest to be crucial in GIP.GIPR interaction. However, the Glu3Pro-GIP lacks the positive charge in position 3, which is important in receptor activation by interaction with Arg183 in TMH2. The comparison between the native GIP (left) and its antagonistic derivative Glu3Pro-GIP (right) clearly indicates that, due to substitution of Glu3 to proline, Arg183 does not interact with the ligand. Instead, Arg183 interacts with Gln384 in TMH7, thus, constraining the receptor in an inactive state.

31

Table: Effect of mutation of human GIPR on its expression and ability to induce cAMP

formation

GIP-R	Location	Receptor Expression[#]	cAMP production		
			$EC_{50} \pm SEM$ (nM)	Fmut[§]	Emax[Φ]
WT		100	1.96 ± 0.32	-	100
Mutant R183A	TMH II	76.1 ± 4.6	149.7 ± 30.8***	76.4	84.2 ± 9.5
Mutant R190A	TMH II	84.9 ± 6.7	139.3 ± 16.8***	71.2	81.7 ± 7.1
Mutant Q220A	TMH III	110.2 ± 1.1	9.2 ± 4.3***	4.7	99.0 ± 7.0
Mutant T223A	TM III	116.9 ± 17.0	6.7 ± 2.6***	3.4	100.3 ± 5.1
Mutant Q224A	TM III	77.2 ± 7.6	11.0 ± 5.0***	5.6	117.0 ± 6.7
Mutant N230A	TM III	91.9 ± 0.7	12.7 ± 1.2***	6.5	98.1 ± 6.8
Mutant Y231A	TM III	102.5 ± 1.7	4.2 ± 0.9*	2.1	114.5 ± 15.2
Mutant Y231F	TM III	96.2 ± 8.1	7.9 ± 4.8**	4.0	101.2 ± 7.8
Mutant R300A	TM V	75.1 ± 6.5	82.3 ± 15.9***	42.0	85.8 ± 3.8
Mutant H353A	TM VI	96.5 ± 8.7	2.5 ± 1.7	1.3	130.9 ± 8.9
Mutant F357A	TM VI	77.0 ± 6.1	30.8 ± 9.3***	15.7	114.1 ± 11.7
Mutant Q384A	TM VII	115.3 ± 3.4	5.2 ± 1.4**	2.6	111.5 ± 23.0
Mutant Q384N	TM VII	109.4 ± 9.7	3.2 ± 1.6	1.6	115.8 ± 15.8
Mutant Y392A	TM VII	89.9 ± 3.9	9.5 ± 4.0***	4.8	106.8 ± 13.2
R1831.Q384A-GIPR	TMII-VII	12.0 ± 0.2	32.5 ± 12.3**	16.6	28.0 ± 10.2

[#] Receptor expression was measured by flow cytometry using GIP-Alexa F 647 as label of

GIPR. Results are expressed as percent of expression value of the WT-GIPR and are the

means SEM of 3-4 individual experiments.

§ corresponds to mutation factor which were calculated as $F_{mut} = EC_{50}$ (mutated GIPR) / EC_{50} (WT-GIPR), with EC_{50} being potency of GIP (based on 4-9 determinations).

Φ corresponds to efficacy of GIP to stimulate cAMP production. Emax values are expressed in percent of GIP-stimulated cAMP production with the WT-GIPR.

* $p < 0.05$, ** $p < 0.01$, *** $p < 0.001$ evaluated by student t-test as compared to wild-type receptor value.

Fig.1

TMH1 GIP-R   V**MY**TVGY**SL**SLATL**LL**ALLIL**SLF**
         Adenosine A2a-R SV**Y**ITVELAIAVLAI**L**GNVLVCWA
         Rhodopsin   SMLAAYMF**L**LIMLGFPINFLTLYV
                                               ^

TMH2 GIP-R   TR**NYI**HI**NL**FTSFMLRAAAILSRDRLLPRP
         Adenosine A2a-R VT**NY**FVVS**L**AAADIAVGVLAIPFAIT**I**STG
         Rhodopsin   PL**NYI**LL**NL**AVADLFMVFGGFTTTLYTSLH
                                             ^

TMH3 GIP-R   LAA**C**RTAQIVTQ**Y**CVGANYTW**LLV**EGVYLHSLL
         Adenosine A2a-R CHG**C**LFIACFVLVLTQSSIFS**LL**AIAIDRYIAI
         Rhodopsin   PTG**C**NLEGFFATLGGEIALWS**L**VVLAIERYVVV
                                                              ^

TMH4 GIP-R   G**H**FRYYLLLGW**G**AP**A**LFVI**P**WVI
         Adenosine A2a-R TRAKGIIAIC**W**VLSFAIGLTPML
         Rhodopsin   N**H**AIM**G**VAFTWVMALACAA**PP**LV
                                ^

TMH5 GIP-R   EVKAIWWIIRTP**I**LMTI**LI**NF**L**IFIR
         Adenosine A2a-R MNYMVYFNFFACV**L**VPL**LL**MLGVYLR
         Rhodopsin   NESFVIYMFVVHFIIPLIVI**FF**CYGQ
                                               ^

TMH6 GIP-R   LARS**T**LT**L**VPLL**G**VHEVVFA**P**VTEEQ
         Adenosine A2a-R EVHAAKS**L**AIIV**G**LFALCWL**P**LHIIN
         Rhodopsin   EKEV**T**RMVIIMVIAFLICWL**P**YAGVA
                                                 ^

TMH7 GIP-R   AKLGFE**IFLS**SFQGFLVS**VLY**
         Adenosine A2a-R WLMYLA**IVL**SHTNSVVNPFIY
         Rhodopsin   IFMTIPA**FF**AKTSAVYNP**VIY**
                                                 ^

Legend	
<u>X</u>	= Similar
X	= Identical
^	= .50

Fig. 2

GIP

TMH1
TMH2
TMH7
TMH3
TMH4
TMH5
TMH6
ECD

GIP

TMH1
TMH2
TMH7
TMH3
TMH4
TMH5
TMH6
ECD
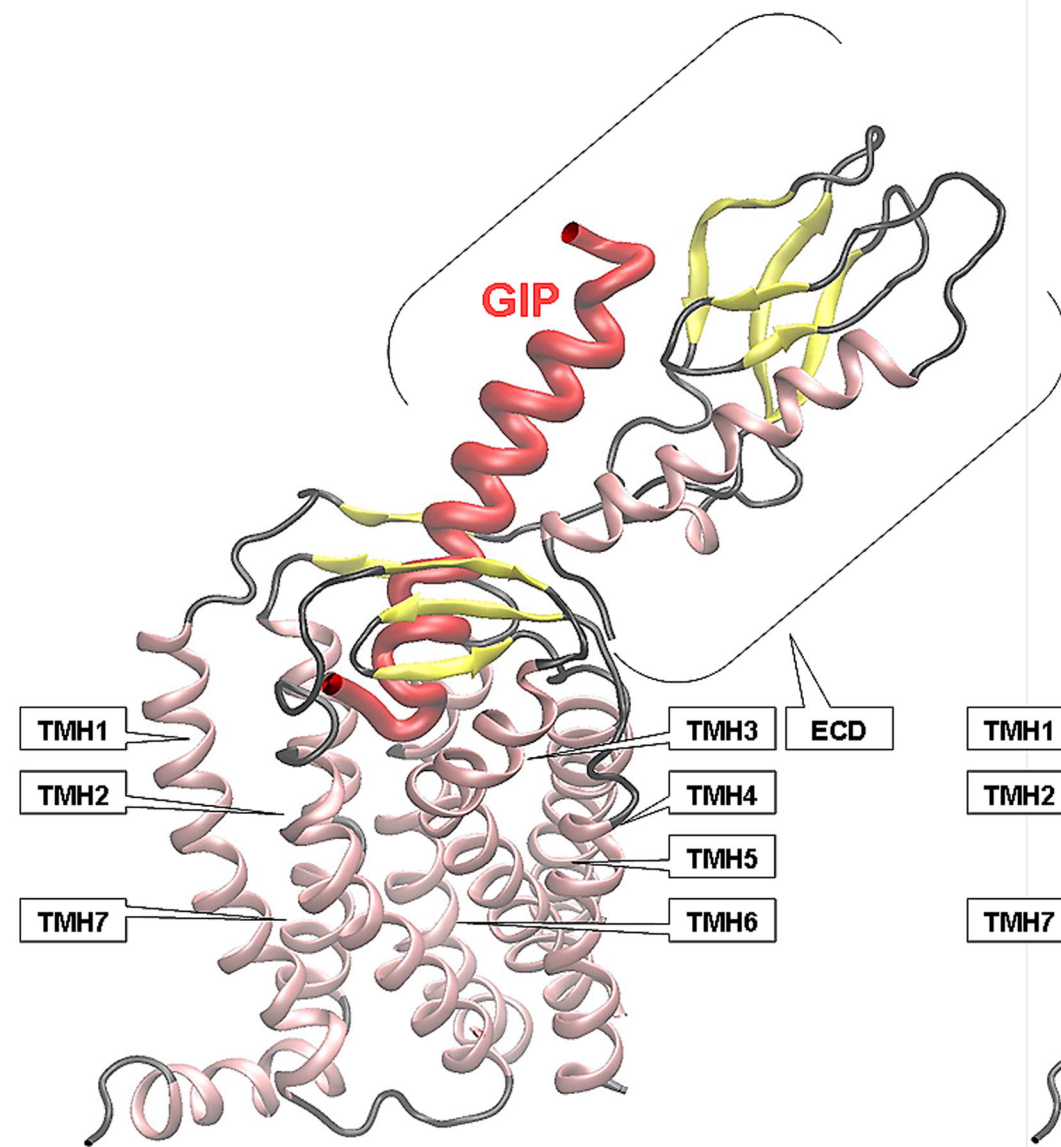
(a) Glucagon-like binding mode
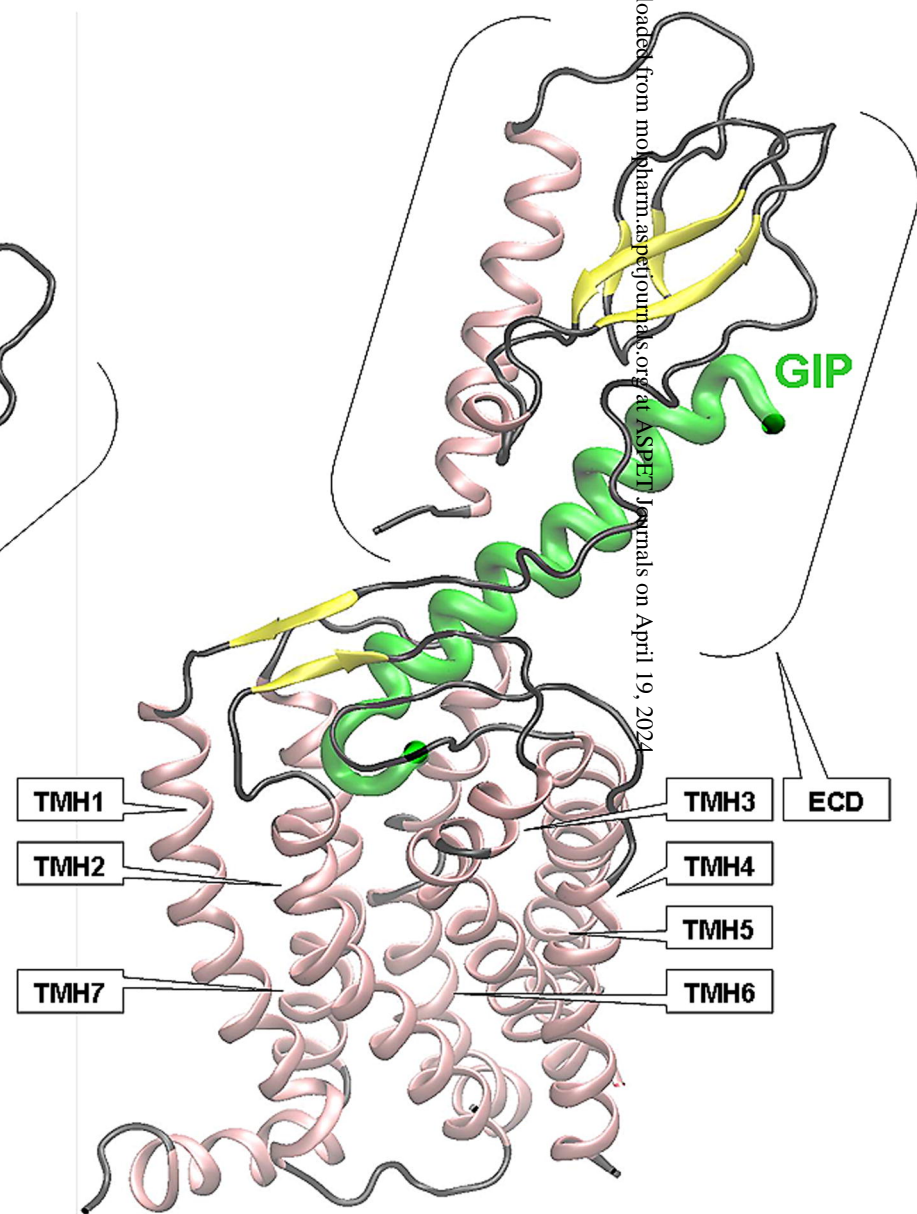
(b) Secretin-like binding mode

Tyr-Ala-Glu-Gly-Thr-Phe-Ile-Ser-Asp-Tyr-Ser-Ile-Ala-Met-Asp-Lys-Ile-His-Gln-Gln-Asp-Phe-

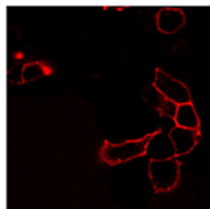Val-Asn-Trp-Leu-Leu-Ala-Glu-Lys-Gly-Lys-Lys-Asn-Asp-Trp-Lys-His-Asn-Ile-Thr-Gln-COOH
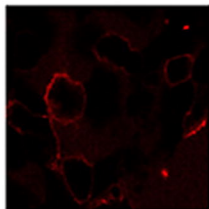
Fig. 3

A)

GIP-Alexa-F 647

B)

GIP

GIP-Alexa-F 647
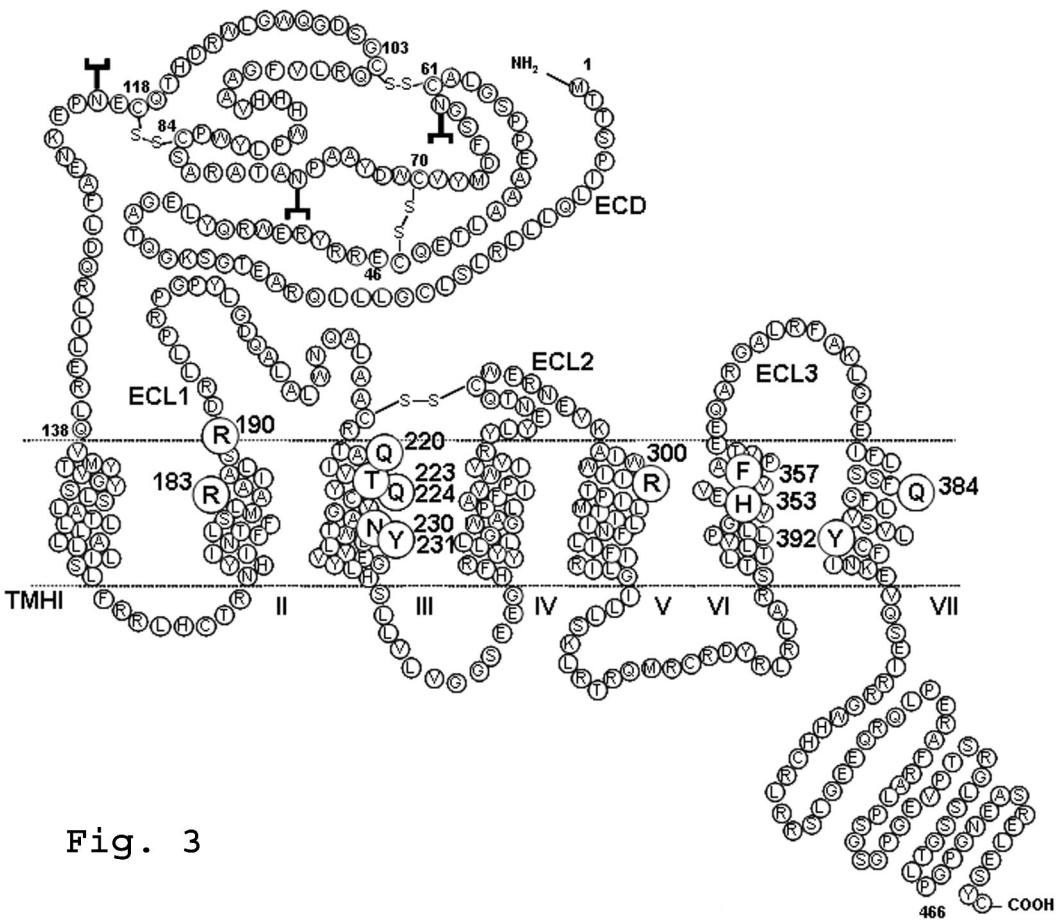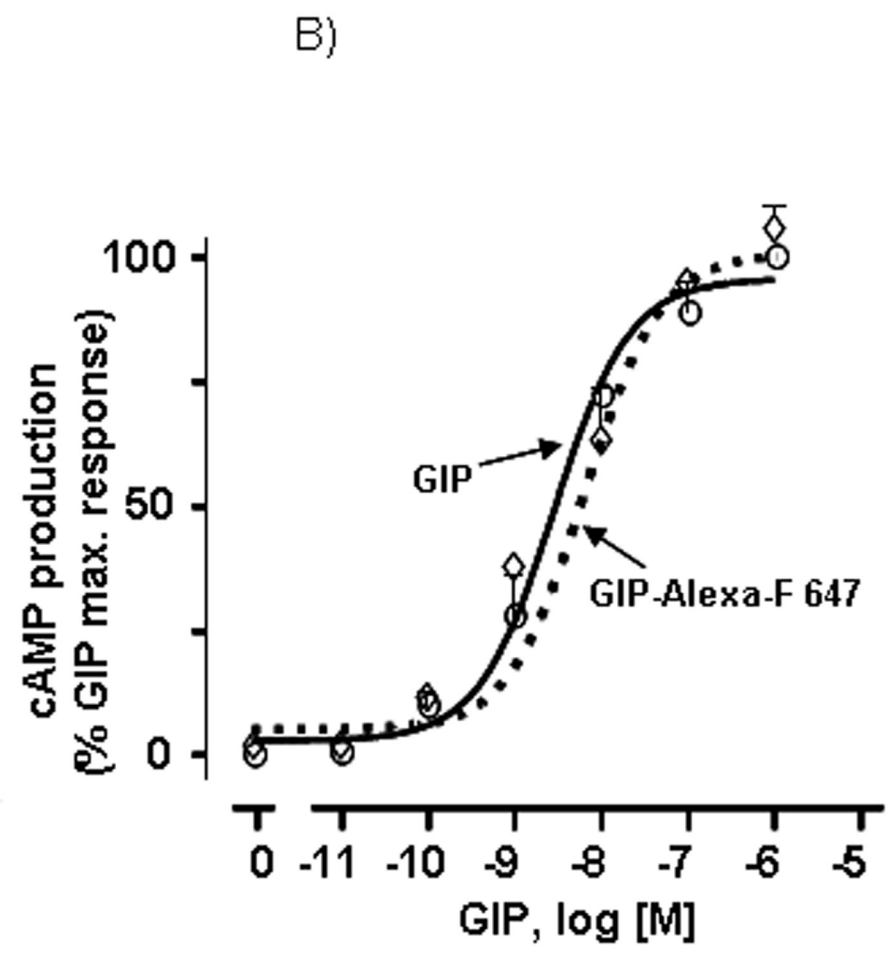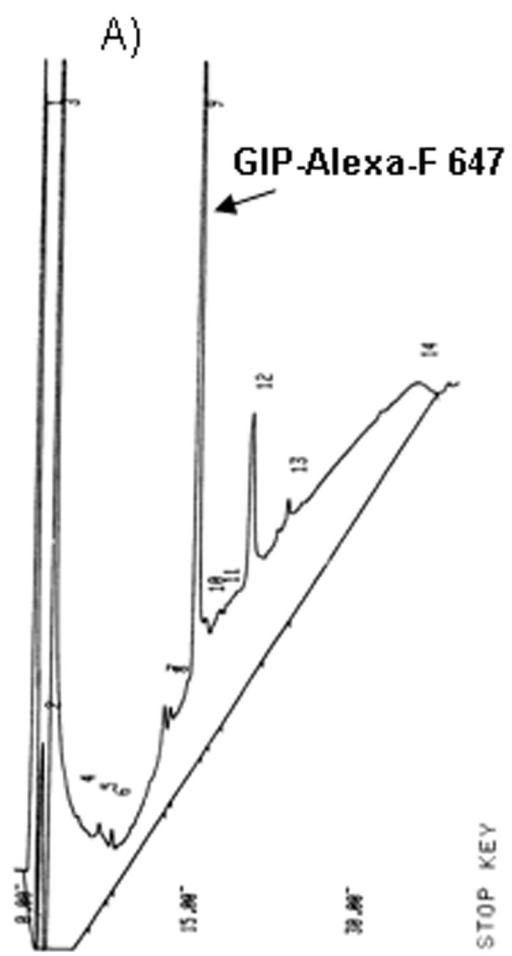
Fig 4

WT-GIP-R R183A-GIP-R Q220A-GIP-R
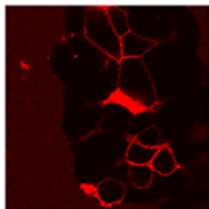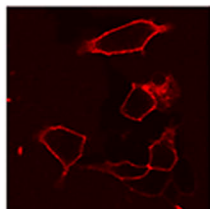
T223A-GIP-R R300A-GIP-R F357A-GIP-R
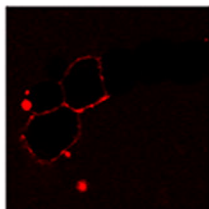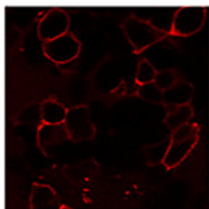
Fig. 5
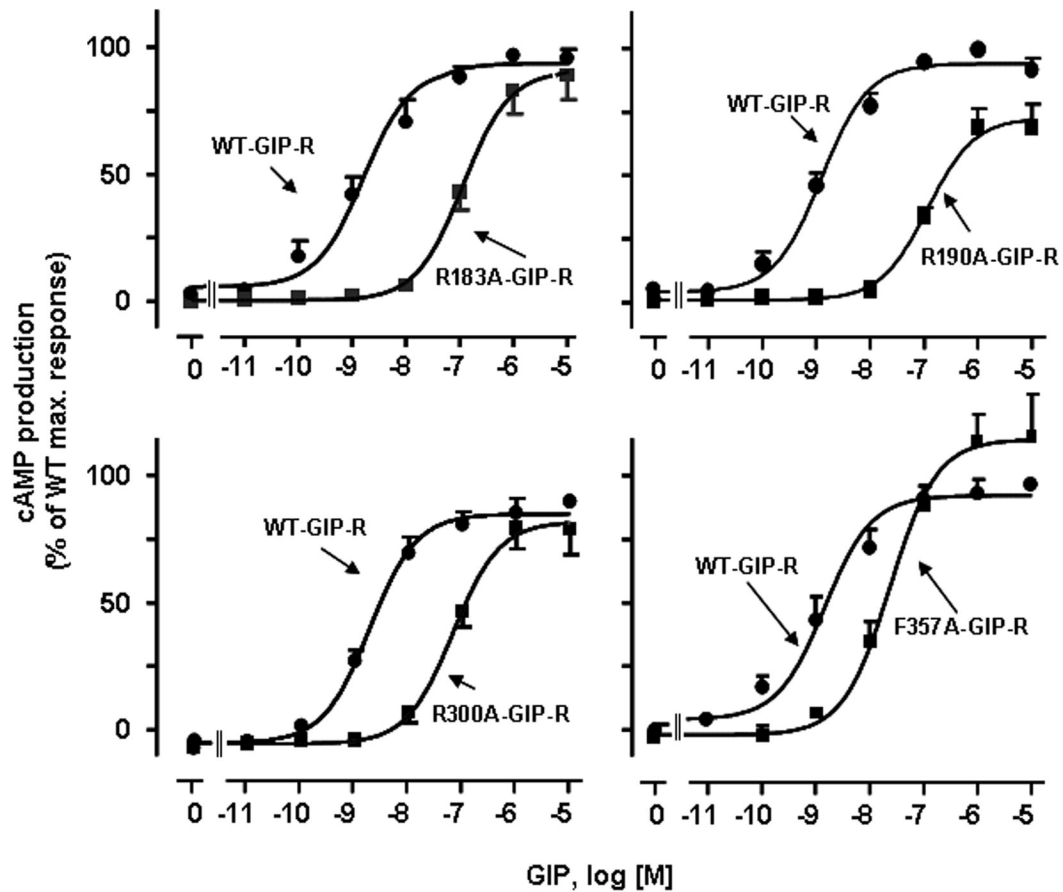
Fig. 6
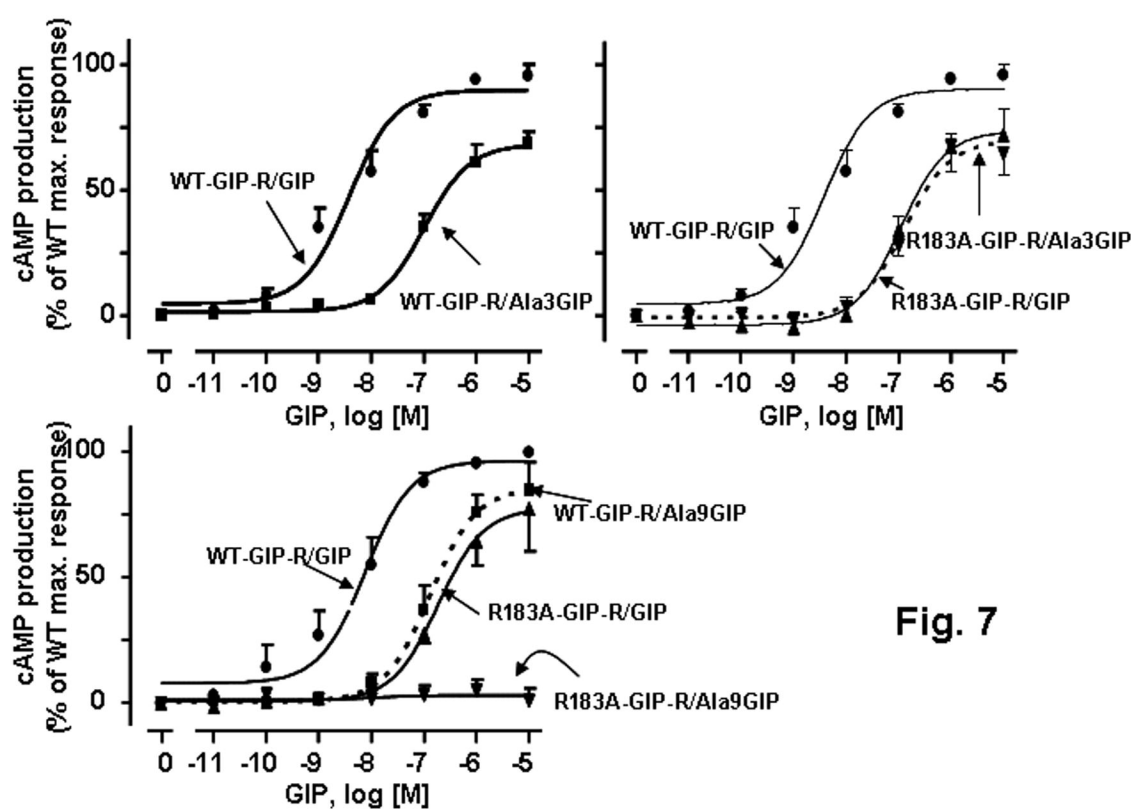
Fig. 7
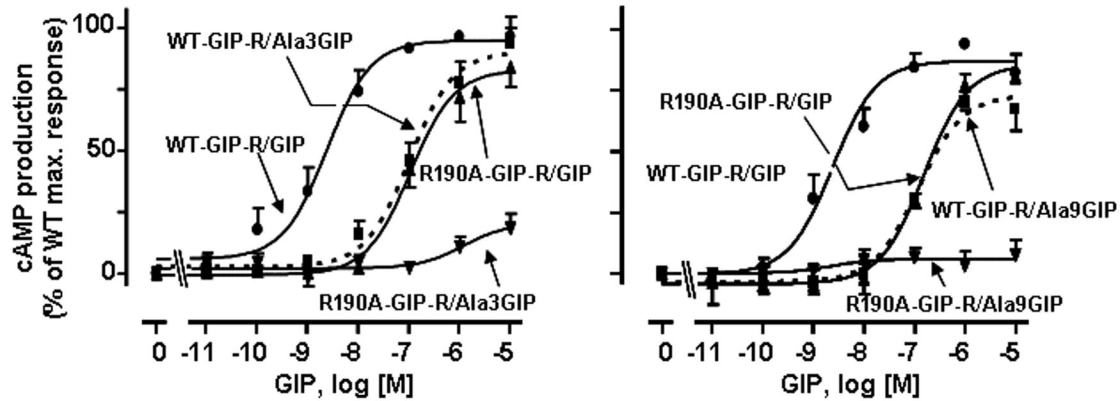
Fig 8

Fig. 9

Fig. 10

Fig. 11

Fig 12